Research Article

Hydrodynamic Modeling of the Roman Harbor of Portus in the Tiber Delta: The Impact of the North-Eastern Channel on Current and Sediment Dynamics

Bertrand Millet,[1]* Hervé Tronchère,[2] and Jean-Philippe Goiran[2]

[1]Mediterranean Institute of Oceanography, UMR 7294 CNRS / Aix-Marseille Université, Marseille, France
[2]Archéorient, UMR 5133 CNRS, Maison de l'Orient et de la Méditerranée, Université de Lyon, Lyon, France

Correspondence
*Corresponding author;
E-mail: bertrand.millet@univ-amu.fr

Received
9 September 2013
Revised
13 February 2014
Accepted
16 February 2014

Scientific editing by Jamie Woodward

Published online in Wiley Online Library (wileyonlinelibrary.com).

doi 10.1002/gea.21485

This study examines the hydrodynamics of the Roman harbor of Portus during the Trajanic period (second century A.D.). We have evaluated the impact of the north-eastern channel on water circulation and sediment resuspension within the harbor in relation to the problem of sediment infilling. We used a 2D numerical model to compute the distribution of the depth-averaged current velocity, bed shear stress, and kinetic energy induced by each of the four prevailing local winds. First, the results confirm the persistent conditions for sediment infilling over the entire western harbor basin, even when the north-eastern channel is operational; these conditions being present for 61.3% (40.3%) of the summer period and up to 68% (44.2%) of the winter period in the south-western harbor basin. Second, the results show that favorable conditions for navigation occur in the central basin, leading to the landing installations, under the S 180°, SE 135°, and NE 22° winds when the north-eastern channel is operational; these conditions being present for 21% of the summer period and 51.3% of the winter period. Inversely, the access to the landing installations with both channels operating remains affected by sediment infilling, for 40.3% of the summer period and 16.7% of the winter period. © 2014 Wiley Periodicals, Inc.

INTRODUCTION

The harbor complex of Portus is located in the Tiber delta, 3 km north of the harbor basin of Ostia (Fea, 1824; Heinzelmann & Martin, 2002; Goiran et al., 2012, 2014). During the first and second centuries A.D., two main phases of reorganization in Portus were carried out (Keay et al., 2005; Keay & Paroli, 2011): the structures built before Trajan's reign, and the additions made during Trajan's reign (Figure 1). The pre-Trajanic structures consist of the two long breakwaters built to enclose the large western basin, constructed between 42 and 52 A.D. during the reign of Claudius, then completed and inaugurated under Nero (64–66 A.D.). This older configuration includes a series of constructions in the south-eastern sector: the *darsena* (a small basin rectangular in shape), a long south–north central pier that bisects the main basin, and a small canal, the Canale Trasverso, that leads to the Tiber and Rome via the Fiumicino canal (present name of the ancient canal of Trajan; Figure 1). This Claudian harbor became the greatest harbor of the ancient Mediterranean world, measuring 200 ha (Morelli, Marinucci, & Arnoldus-Huyzendveld, 2011) and protected by the two long north-western and south-western breakwaters. However, it may be that this older harbor was inefficient, as we know from Tacitus that 200 ships were destroyed in the Claudian harbor by a storm in 62 A.D. (Tacitus, Annales, XV, 18). It is still debatable why Trajan decided to dig a new basin and transform the Claudian harbor, only 40 years after it had been inaugurated. One argument is that the Claudian harbor may have been too exposed to storms and currents; another is that the harbor may have been rapidly infilled by sediment deposition (Le Gall, 1957; Zevi, 2001).

A second building phase during Trajan's reign included the construction of the well-protected hexagonal basin (built between 100 and 112 A.D.) with quays 357 m long and a total area of 33 ha, the reorganization of several

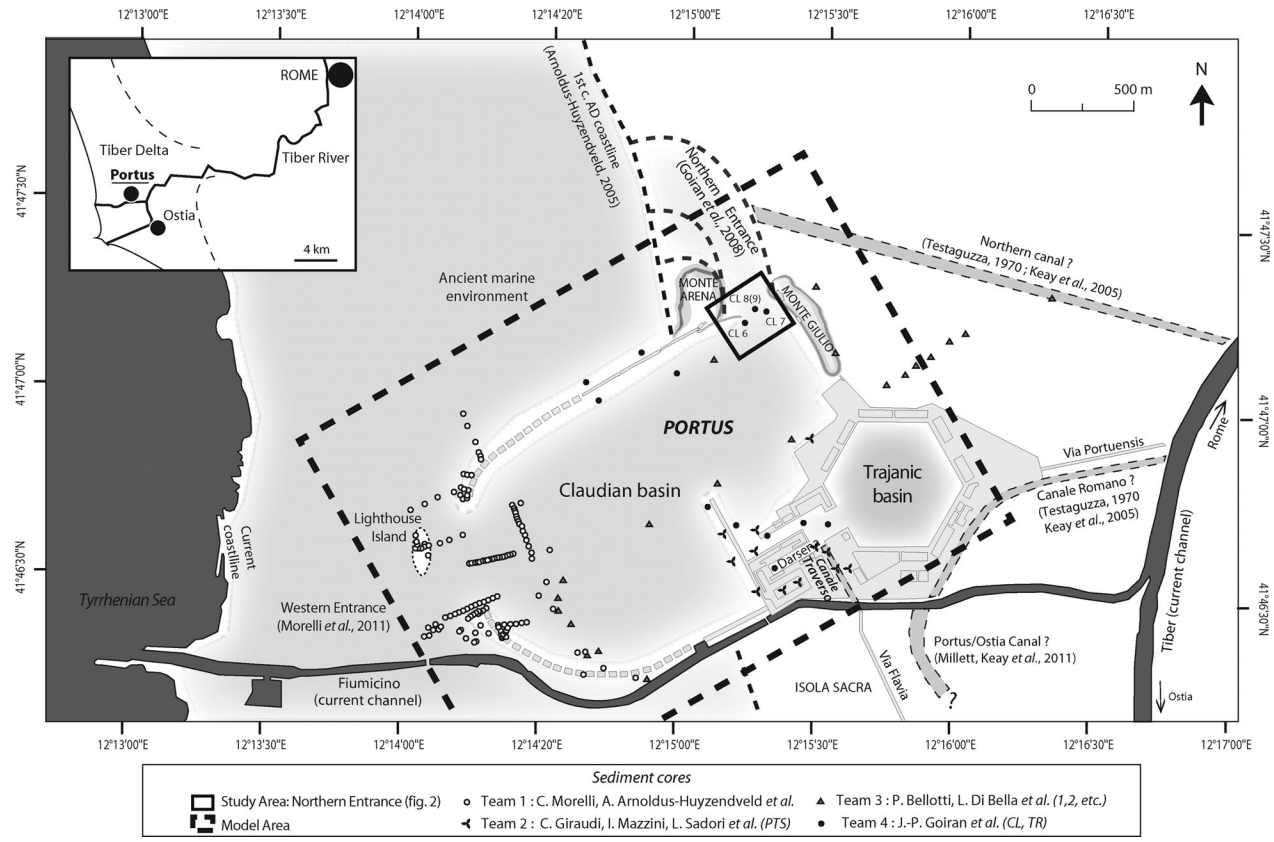

Figure 1 Configuration of the harbor of Portus during the Trajanic period with locations of sediment cores.

Portus districts, and perhaps the opening of the secondary north-eastern channel (Figure 1). The so-called harbor of Portus consists of both the pre-Trajanic installations (mainly the huge basin of Claudius' reign) and the reorganization carried out during Trajan's reign. Because of this new inner basin and the further improvements during the second century A.D., the new Trajanic harbor configuration provided more capacity for the mooring of ships and a better system for processing cargoes from seagoing ships, for storage, and for transshipment onto river craft for the journey to Rome.

The present paper presents a set of results from a modeling exercise undertaken to provide new insights into the wind-induced hydrodynamics and sediment resuspension within the Portus, related to the prevailing wind conditions. The model was applied to the two different configurations of the harbor: first, the western channel, and second, both the western and north-eastern channels. In each configuration, the model computes the wind-induced current velocities, the bed shear stresses, and the kinetic energies of the water masses, which are proxies for sediment resuspension and transport. Strong (weak) values of bed shear stress associated with high (low) levels of kinetic energy can be representative of a resuspension (deposition) area for sediment particles. In addition, medium levels of kinetic energy associated with very weak values of bed shear stress can be representative of an area in which sediment is transported by the water masses.

This approach leads to a comparative study of the relative efficiency of the harbor according to these different configurations, in the context of the prevention of sediment infilling of the inner landing structures. The interpretations of the results especially focus on the impact of the north-eastern channel on the circulation of water masses and sediment dynamics within the harbor basins and inner areas. Hypotheses may thus be proposed that justify either the opening or the improvement of this secondary north-eastern channel in relation to the following question: was it very important for the Roman engineers to manage this north-eastern channel in relation to the sediment infilling of the harbor?

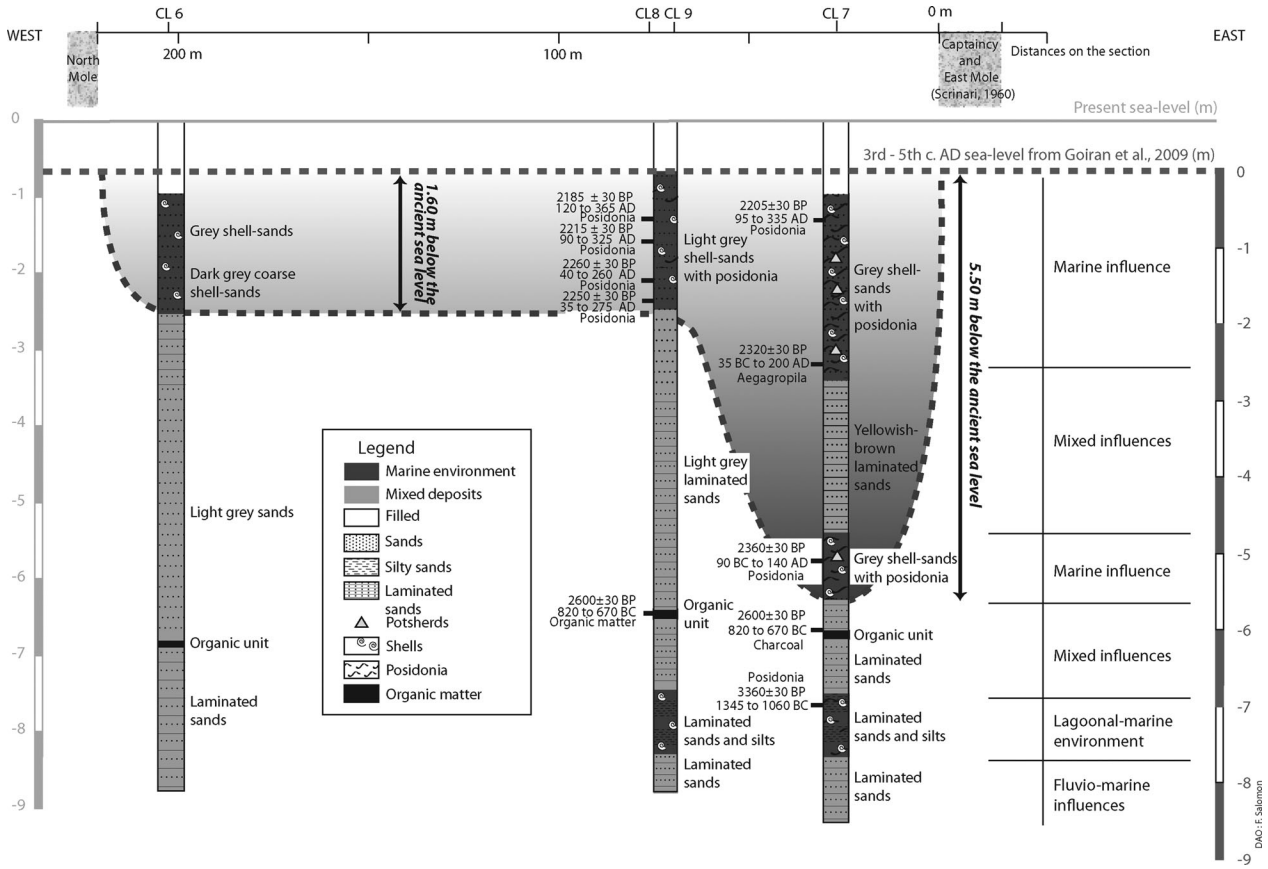

Figure 2 Stratigraphic cross-section of the north-eastern channel of Portus and details of the locations of cores.

METHODS

Cores from the North-Eastern Channel

Figure 2 presents the data from several sediment records that were obtained by drilling in the north-eastern part of the harbor, between the known eastern extremity of the breakwater and the archaeological remains on Monte Giulio, in order to assess the existence of a hypothetical channel (Lugli & Filibeck, 1935; Testaguzza, 1970; Goiran et al., 2011a). Boreholes 6, 7, 8, and 9 revealed the presence of a thick layer of marine deposits, characterized by the abundant presence of sea-shells and posidonia. The sediment texture was quite coarse and well-sorted that indicates strong flows and currents; mean grain sizes ranged between 250 and 500 μm, and histograms of granulometry presented unimodal profiles (Goiran et al., 2011b). Combined with the broken sea-shells, this suggests a strong hydrodynamic context compatible with an operating channel. Thanks to the determination of the Roman sea level by Goiran et al. (2009) from biological investigations performed on the piers of the harbor of Portus, it is possible to directly quantify the depths of the basins from sediment cores. The depth of the channel reached 5.5 m below the ancient sea level in borehole 7, which was more than enough to allow the navigation of high-sea ships (Boetto, 2010). The channel was shallower in its western part with a maximum of 1.6 m depth. All types of vessels could access the inner basin by the 5.5 m channel; one of the largest Roman wrecks excavated (70–65 B.C.), discovered at Madrague de Giens near Hyères in southern France in 1967, may have been a ship that used this channel. This ship, 40 m long and 9 m wide with a 4.5 m wedge depth, had a capacity of 400 tons deadweight with a displacement of about 500 tons, and its draft at full load was estimated between 3.5 and 3.7 m (Pomey & Tchernia, 1978; Pomey, 1982, 1997).

The zone of the north-eastern channel presented a very high sediment deposition rate. At least at the beginning of the third century A.D., the channel did not exceed 2.5 m in depth, and it is possible that navigation was no longer possible, at least in the middle of the fourth century A.D. when the channel became shallower than 0.5 m. It is likely that the north-eastern channel was periodically dredged, but it remains very difficult to confirm

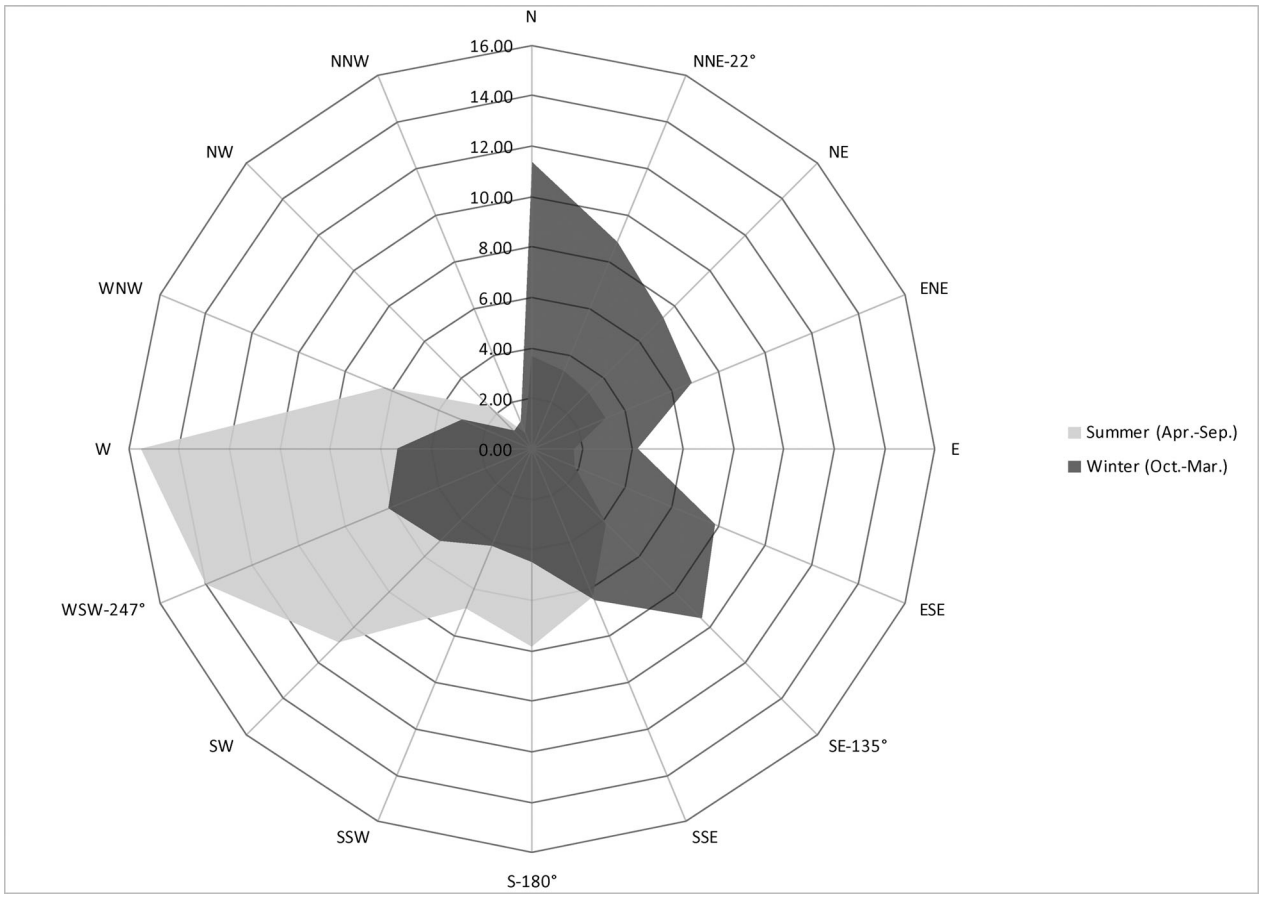

Figure 3 Wind rose of interannual wind measurements at the meteorological station of Fiumicino airport showing summer winds (April–September) and winter winds (October–March), with corresponding frequencies of occurrence (%).

such events from sediment cores (Morhange & Marriner, 2009; Marriner, Morhange, & Goiran, 2010; Stanley & Bernasconi, 2012; Özdaş & Kızıldağ, 2013). In addition, the margin of error of the radiocarbon dating (before or during the Trajanic period) does not allow us to establish whether this north-eastern channel was built during the pre-Trajanic or the Trajanic period.

A numerical model was applied to a bathymetric map derived from the water depths observed in the boreholes (Giraudi et al., 2006; Bellotti et al., 2007, 2011; Giraudi, Tata, & Paroli, 2009; Goiran et al., 2010, 2011a,2011b; Morelli, Marinucci, & Arnoldus-Huyzendveld, 2011). The base of the deepest marine-like deposits, lying on the top of older fluvial deposits brought by the Tiber, was used as the harbor depth reference to interpolate the bathymetric map. Where available, radiocarbon dates were also used to ascertain the depths at the period of the harbor construction. The data were supplemented by the results published by other scientists that provided new insights into the morphology of the pre-Trajanic harbor basin (Arnoldus-Huyzendveld, 2005; Sadori et al., 2010; Di Bella et al., 2011; Mazzini et al., 2011; Morelli, Marinucci, & Arnoldus-Huyzendveld, 2011; Pepe et al., 2012). Radiocarbon dates obtained in this zone as part of the MEFRA (*Les Mélanges de l'École Française de Rome—Antiquité*) Project, and the related information concerning the methods of analysis used in processing the samples, were presented in a previous paper (Goiran et al., 2011a).

Local Wind Regime

The local wind regime was obtained from the interannual wind statistics available at the meteorological station of Fiumicino airport; Figure 3 presents the corresponding frequencies of occurrence of the seasonal wind directions, separately considered for the winter (from October to March) and the summer (from April to September) periods. Assuming that the wind regime in the Trajanic period was the same as today, we estimated that the local wind regime could be characterized by four

prevailing wind directions, centered on sectors NNE 22°, SE 135°, S 180°, and WSW 247° (Figure 3). The dominant winds considered to be representative for the summer period (April–September), the most favorable season for navigation, are the SW 247° and S 180° winds, with seasonal frequencies of occurrence of 40.3% and 21%, respectively. The dominant winds considered to be representative for the winter period (October–March), the weaker period for harbor activity (Pomey & Tchernia, 1978; Pomey, 1982, 1997), are the NE 22°, SE 135° winds and again, the SW 247° wind, with seasonal frequencies of occurrence of 27.5%, 23.8% and 16.7%, respectively. The instability of the wind direction on either side of each prevailing wind sector, over an angle of 45°, was taken into account in computing each frequency of occurrence mentioned above as the sum of three frequencies, corresponding to the frequency of the central sector mentioned above and those of both adjacent sectors. We used in all computations a constant wind intensity of 8 $m \cdot s^{-1}$, which was considered from observations to be a representative value of the mean local wind regime.

Numerical model

We used a bidimensional-horizontal (2D-H) numerical model to resolve the depth-integrated equations of the fluid dynamics, previously used for the ancient harbors of Lacydon (Millet, Blanc, & Morhange, 2000) and Alexandria (Millet & Goiran, 2007). This application was in good agreement with the shallow bathymetry of the Portus harbor (9 m maximum depth), and the approximation of a well-mixed coastal system with constant water density $\rho = 1027$ $kg \cdot m^{-3}$. The equations are the followings:

$$\delta U/\delta t + U\delta U/\delta x + V\delta U/\delta y = fV - g\delta\zeta/\delta x + \tau_{sx}/\rho h - \tau_{bx}/\rho h$$

$$\delta V/\delta t + U\delta V/\delta x + V\delta V/\delta y = -fU - g\delta\zeta/\delta y + \tau_{sy}/\rho h - \tau_{by}/\rho h$$

$$\delta\zeta/\delta t + \delta(hU)/\delta x + \delta(hV)/\delta y = 0$$

where t, x, and y, the time and space index according to both horizontal directions; U and V, the horizontal components of the vertical averaged current velocity ($cm \cdot s^{-1}$); f, the Coriolis parameter and g, the gravity; ζ, the surface elevation; h, the water depth of each mesh of the grid; τ_{sx} and $\tau_{sy,}$ the horizontal components of the wind stress at the water surface ($N \cdot m^{-2}$):

$\tau_{sx} = \rho_a \cdot C_d \cdot W^2 \cdot \sin\alpha$ and $\tau_{sy} = \rho_a \cdot C_d \cdot W^2 \cdot \cos\alpha$

with W and α, the wind velocity and direction; ρ_a, the air density; and C_d, the drag coefficient of the wind ($C_d = 3.5 \times 10^{-3}$).

τ_{bx} and τ_{by}, the horizontal components of the current-induced bed shear stress ($cN \cdot m^{-2}$): $\tau_{bx} = \rho \cdot g \cdot U(U^2 + V^2)^{0.5}/C^2$ and $\tau_{by} = \rho \cdot g \cdot V(U^2 + V^2)^{0.5}/C^2$

with C, the Chézy coefficient ($m^{0.5} \cdot s^{-2}$) for bed shear stress, computed according to the water depth: $C = 40h^{1/6}$. In addition, the kinetic energy E_k ($J \cdot m^{-3}$) corresponding to the flowing water masses was computed, following the equation: $E_k = 0.5\rho(U^2 + V^2)$.

The 2D-H model was applied to the Trajanic harbor by using a 166 × 167 grid of regular 25 m square meshes and a time-step of 1 second. The model operated by considering successively two sets of computations, applied to the one-channel and the two-channel configurations, respectively. The model computed at steady state both the depth-averaged current velocities and the fields of bed shear stress and kinetic energy, successively induced by each wind direction of the local wind regime. In addition, the model took into account the water circulation inside the downstream section of the Fossa Traiana and the Canale Trasverso. The circulation inside these channels was induced in each computation by the slope of the water surface, controlled by the water levels computed by the model at each downstream channel extremity and a constant water level heightening of 10 cm defined at the upstream limit of the Canale Trasverso.

RESULTS

Dynamics within the One-Channel Harbor Configuration

Figure 4 presents the superposition of the bathymetry field of the one-channel harbor configuration and the depth-averaged current vectors computed under the four prevailing winds, with consideration of the additional water circulation inside the Canale Trasverso and the Fossa Traiana. The results show that the hydrodynamic pattern within the western harbor basin is characterized by one large anticlockwise eddy according to the SW 247°, S 180°, and SE 135° (NE 22°) winds, whereas hydrodynamic patterns within the eastern sector are characterized by small adjacent eddies flowing in opposite directions depending on the winds. Table I compares the maximum values of current velocity reached at different locations within the harbor (NW, SW, NE, and along the central pier) depending on the wind direction. The highest currents are located along the eastern breakwater and the central pier whatever the wind direction, up to 21.7 $cm \cdot s^{-1}$ being reached under the NE 22° wind, and the lowest currents ranging below 8.1 $cm \cdot s^{-1}$ occur in the western harbor basin under the SW 247° wind. In addition, the results show that the fluxes exchanged

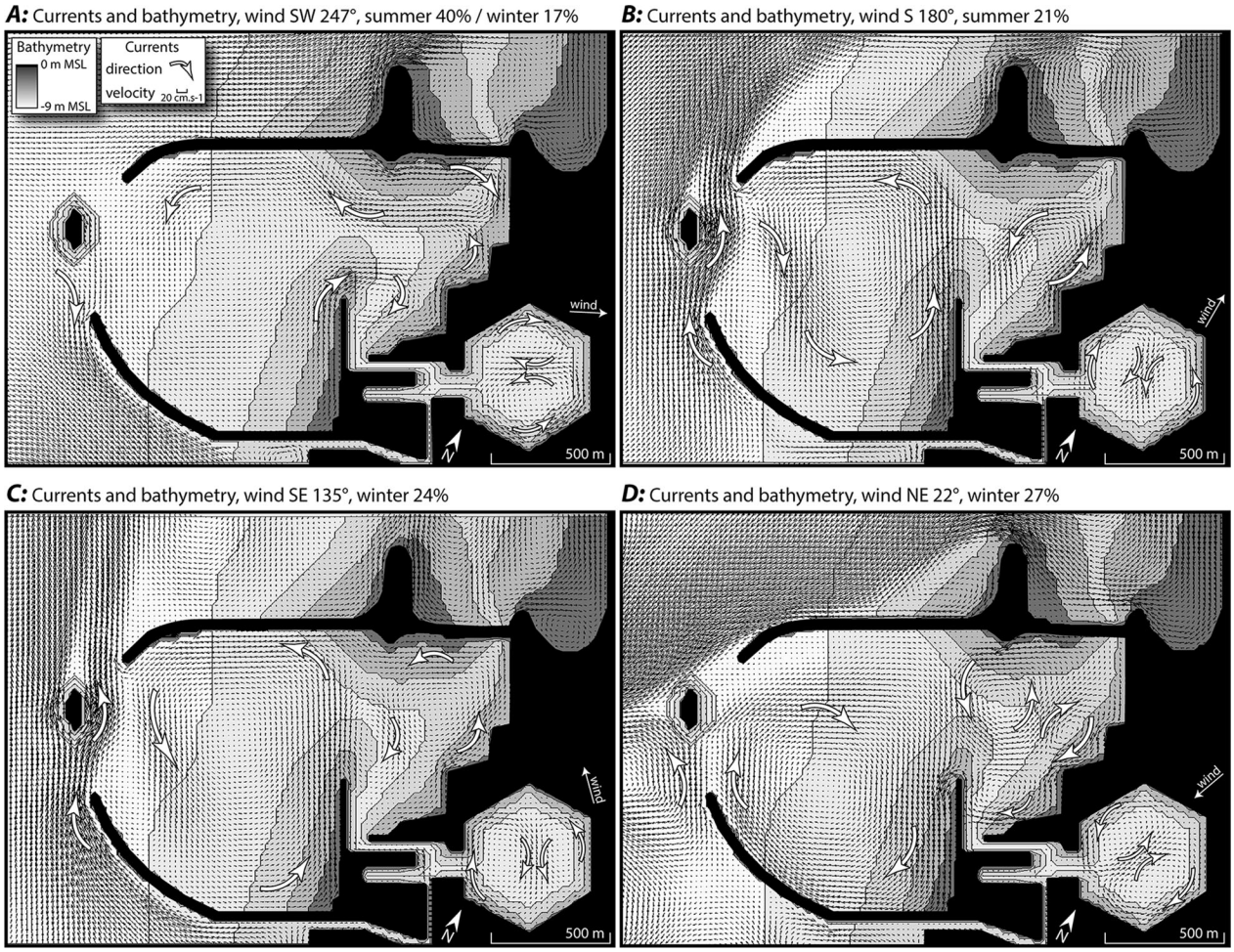

Figure 4 Modeling of the harbor of Portus: bathymetry field (m) of the one-channel configuration and depth-averaged current velocities ($cm \cdot s^{-1}$) computed under the prevailing local winds—(A) SW 247°, (B) S 180°, (C) SE 135°, and (D) NE 22°—and taking into consideration the water circulation in the Canale Trasverso and the Fossa Traiana.

Table I Spatial distribution of the maximum current velocities ($cm \cdot s^{-1}$) computed in the harbor of Portus for the one-channel configuration, according to the prevailing local winds.

Maximum Current Velocity ($cm \cdot s^{-1}$)	South-West	North-West	North-East	Central Pier
SW 247°	4.3	8.1	19	16.2
S 180°	12.7	14.2	13.2	20.7
SE 135°	11.8	13.7	9.4	19.4
NE 22°	17.1	11.1	21.3	21.7

between the harbor basin and offshore areas are close to zero under the most frequent SW 247° wind, and remain very weak for the three other winds, with inflow (outflow) always occurring through the south-western (north-western) channel.

Figure 5 presents the superposition of the kinetic energy field and the bed shear stress vectors computed within the one-channel harbor configuration under the four prevailing winds and in consideration of the water circulation inside the Canale Trasverso and the Fossa Traiana. Table II compares the maximum values of bed shear stress and kinetic energy reached at different locations within the harbor, depending on the wind direction. These computed hydrodynamic patterns that fit closely with the sediment dynamics (resuspension, transport, and deposition) of sand-sized particles throughout the harbor are no longer characterized by eddies, but here present contrasted areas of adjacent strong (longer black arrows) or weak (shorter black arrows) values of bed shear stress, and high (white patches) or low (dark patches) values of kinetic energy. The results emphasize

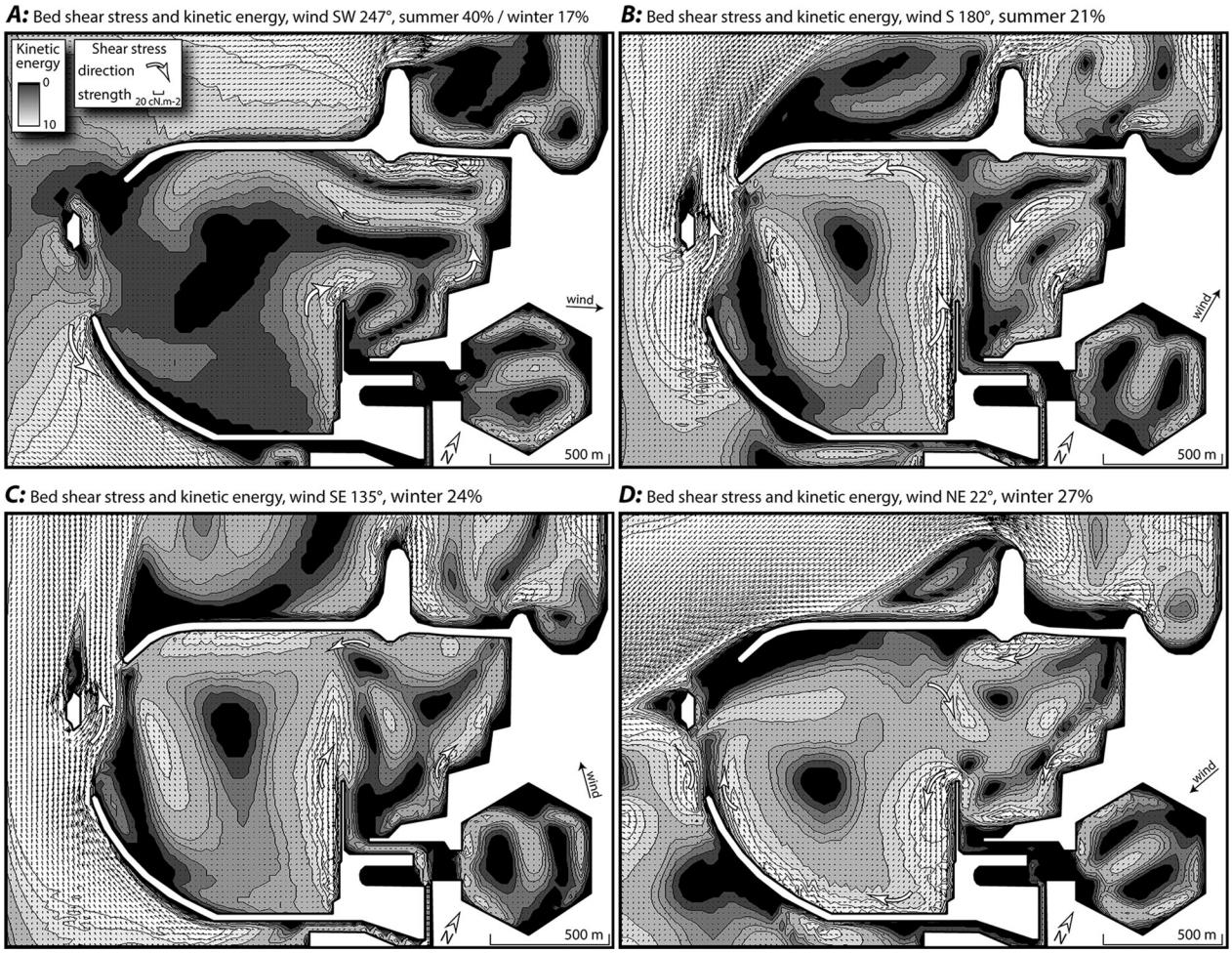

Figure 5 Modeling of the harbor of Portus: kinetic energy field ($J \cdot m^{-3}$) and bed shear stress vectors ($N \cdot m^{-2}$) computed for the one-channel configuration under the prevailing local winds—(A) SW 247°, (B) S 180°, (C) SE 135°, and (D) NE 22°—and taking into consideration the water circulation in the Canale Trasverso and the Fossa Traiana.

Table II Spatial distribution of maximum values of kinetic energy ($J \cdot m^{-3}$) and *bed shear stress* ($cN \cdot m^{-2}$) computed for the one-channel configuration in the harbor of Portus, according to the prevailing local winds.

Kinetic Energy/*Bed Stress* ($J \cdot m^{-3}$)/(*$cN \cdot m^{-2}$*)	South-West	North-West	North-East	Central Pier
SW 247°	1.0/*0.61*	3.4/*2.15*	18.6/*19.3*	13.4/*13.1*
S 180°	8.3/*5.0*	10.4/*6.6*	8.9/*6.3*	22.1/*21.4*
SE 135°	7.2/*4.39*	9.8/*6.35*	5.1/*4.95*	19.4/*18.9*
NE 22°	15.0/*9.6*	5.8/*3.54*	23.3/*22.6*	27.5/*26.6*

that whatever the wind direction, the maximum values of bed shear stress and kinetic energy are located along the western side of the central pier and along the eastern breakwater. In addition, it is noteworthy that the SW 247° and NE 22° (S 180° and SE 135°) winds induce secondary peaks of kinetic energy along the north-eastern (north-western) shore, and that only the NE 22° wind induces high energies along the south-western breakwater.

Table II shows that the highest values of bed shear stress (kinetic energy) ranged from 26.6 $cN \cdot m^{-2}$ (27.5 $J \cdot m^{-3}$), along the central pier under the NE 22° wind, to 0.61 $cN \cdot m^{-2}$ (1.0 $J \cdot m^{-3}$) in the western harbor under the SW 247° wind. Therefore, the results in Figure 5 and Table II show that the areas of prevailing sediment erosion (strong bed shear stress associated with high kinetic energy) are mostly located in the central basin, in the vicinity of the central pier, and along the eastern and north-eastern breakwaters. Inversely, areas of prevailing sediment deposition, featured by low kinetic energy and dark patches in Figure 5, are essentially located in the western basin whatever the wind, and especially in the eddy centers where both currents and

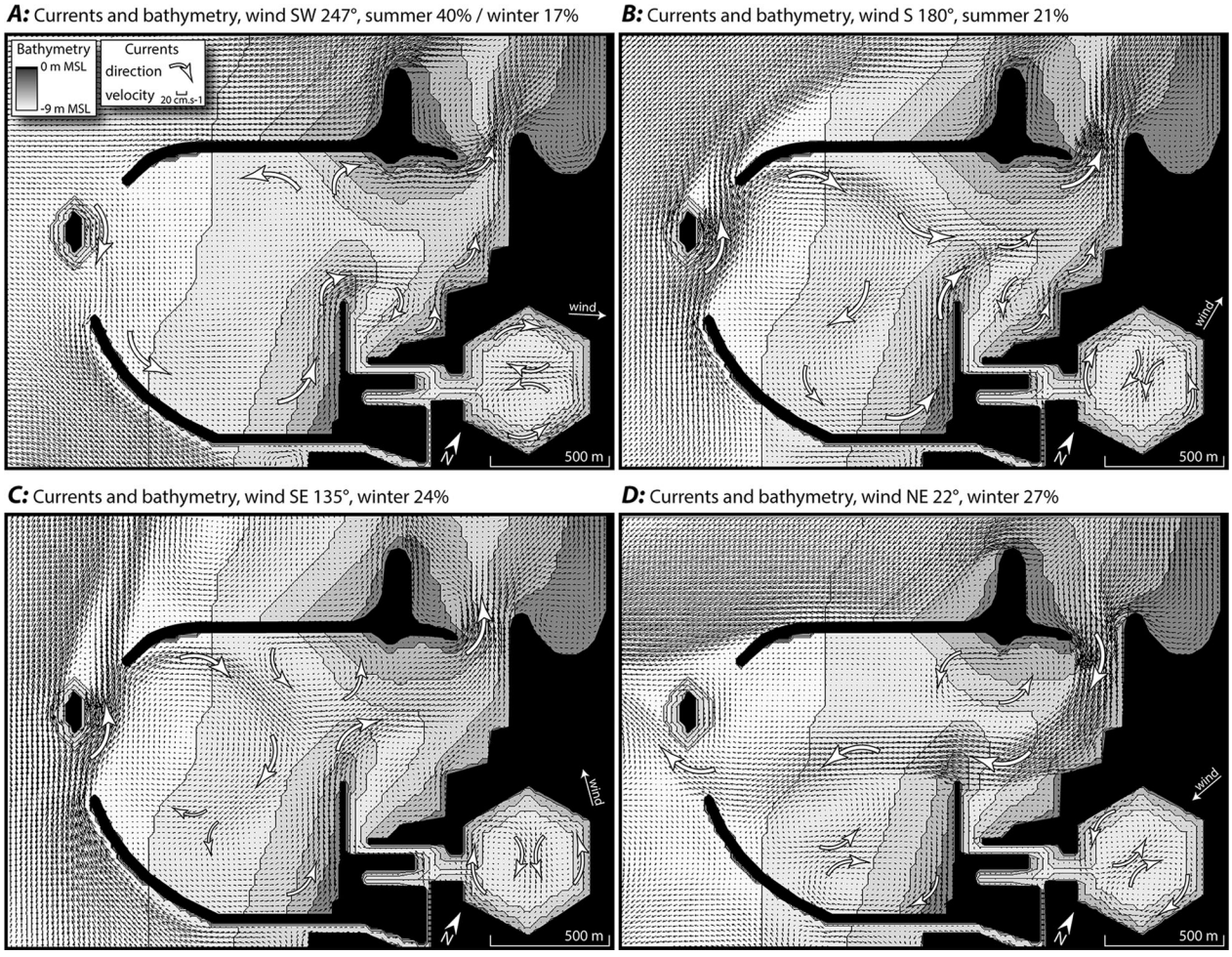

Figure 6 Modeling of the harbor of Portus: bathymetry field (m) of the two-channel configuration and depth-averaged current velocities ($cm{\cdot}s^{-1}$) computed under the prevailing local winds—(A) SW 247°, (B) S 180°, (C) SE 135°, and (D) NE 22°—and taking into consideration the water circulation in the Canale Trasverso and the Fossa Traiana.

energies remain weak. Moreover, the sediment deposition is reinforced under the dominant SW 247° wind, which induces larger patches of weaker energy than the other winds, in the center of both the western and the eastern harbor basins (Figure 4A). Thus, the results confirm that the whole western harbor basin, "artificially" considered through the model with a one-channel configuration, presents a risk of sediment infilling whatever the wind direction, accounting for 61.3% of the summer period and 68% of the winter period. In addition, the results emphasize that the access to the central channel leading to the inner landing installations close to the hexagon is characterized by a context of sediment erosion only under both S 180° and SE 135° winds, accounting for 21% of the summer period and 23.8% of the winter period. These situations of sediment erosion within the central channel are associated with inflowing currents from the Canale Trasverso of 12.3 $cm{\cdot}s^{-1}$ and 16.5 $cm{\cdot}s^{-1}$, related to the S 180° and SE 135° winds, respectively. Inversely, the access to the inner basins presents a high risk of sediment infilling under both the NE 22° and SW 247° winds, accounting for 40.3% of the summer period and 44.2% of the winter period. These situations of sediment deposition are associated with outflowing currents into the Canale Trasverso of 6.1 $cm{\cdot}s^{-1}$ (NE 22° wind) and 3.9 $cm{\cdot}s^{-1}$ (SW 247° wind).

Dynamics within the Two-Channel Harbor Configuration

Figure 6 presents the superposition of the bathymetry field of the two-channel harbor configuration and the depth-averaged current vectors computed under the four prevailing winds, and still with consideration of the

Table III Spatial distribution of the maximum current velocities ($cm \cdot s^{-1}$) computed for the two-channel configuration in the harbor of Portus, according to the prevailing local winds.

Maximum Current Velocity ($cm \cdot s^{-1}$)	South-West	North-West	North-East	Central Pier
SW 247°	4.2	3.6	22.7	13.7
S 180°	9.6	19.6	40.0	20.5
SE 135°	9.8	19.9	33.7	17.9
NE 22°	17.8	3.4	42.2	36.8

additional water circulation inside the Canale Trasverso and the Fossa Traiana channels. In this situation, the circulation pattern still presents eddies as shown in Figure 5, but is here essentially characterized, whatever the wind, by a strong circulation flowing across the entire harbor between the two channels. This cross-circulation is oriented with inflow (outflow) currents passing through the western (north-eastern) channel under the SW 247°, S 180°, and SE 135° winds (Figure 5A, B, and C), and inversely under the NE 22° wind with inflow (outflow) currents passing through the north-eastern (western) channel (Figure 5D). Table III compares the maximum values of current velocity reached at different locations within the harbor, depending on the wind direction. The strongest currents are located in the north-eastern harbor basin or in the vicinity of the north-eastern channel whatever the wind direction, up to 42.2 $cm \cdot s^{-1}$ reached under the NE 22° wind, and the weakest currents, ranging below 3.6 $cm \cdot s^{-1}$, occur in the western sector under the SW 247° wind. In addition, the results show enhanced fluxes exchanged between the harbor basin and

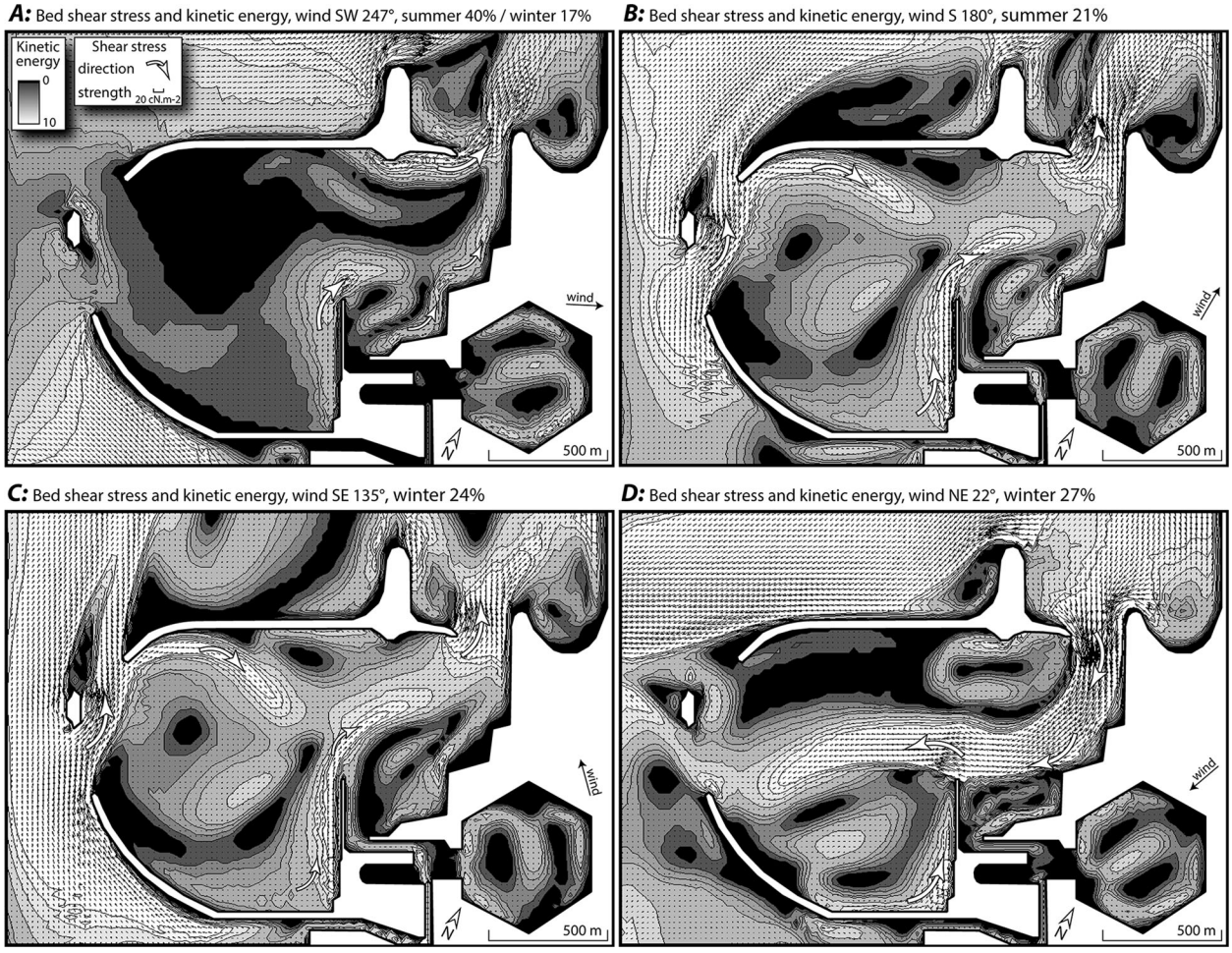

Figure 7 Modeling of the harbor of Portus: kinetic energy field ($J \cdot m^{-3}$) and bed shear stress vectors ($N \cdot m^{-2}$) computed for the two-channel configuration under the prevailing local winds— (A) SW 247°, (B) S 180°, (C) SE 135°, and (D) NE 22°—and taking into consideration the water circulation in the Canale Trasverso and the Fossa Traiana.

Table IV Spatial distribution of maximum values of kinetic energy ($J \cdot m^{-3}$) and *bed shear stress* ($cN \cdot m^{-2}$) computed for the two-channel configuration in the harbor of Portus, according to the prevailing local winds.

Kinetic Energy/*Bed Stress* ($J \cdot m^{-3}$)/($cN \cdot m^{-2}$)	South-West	North-West	North-East	Central Pier
SW 247°	0.9/*0.57*	0.1/*0.1*	26.5/*28.4*	15.6/*15.2*
S 180°	4.8/*3.16*	18.0/*11.0*	82.3/*88.0*	21.5/*20.1*
SE 135°	4.9/*3.25*	17.0/*10.2*	58.4/*62.5*	16.6/*17.9*
NE 22°	5.6/*3.69*	0.9/*0.51*	91.3/*93.6*	69.6/*67.8*

offshore areas, especially through the north-eastern and the south-western channels, with a seasonal variability depending on the winds. The model computed maximum inflow (outflow) currents of 14.1 $cm \cdot s^{-1}$ (21.6 $cm \cdot s^{-1}$), 19.6 $cm \cdot s^{-1}$ (32.8 $cm \cdot s^{-1}$), 21.5 $cm \cdot s^{-1}$ (27.6 $cm \cdot s^{-1}$), and 46.6 $cm \cdot s^{-1}$ (16.3 $cm \cdot s^{-1}$), according to the SW 247°, S 180°, SE 135°, and NE 22° winds, respectively. It is noteworthy that the circulation inside the hexagon is characterized, whatever the wind direction, by relatively strong currents that reach under the SW 247° wind maximum velocities of 8.9 $cm \cdot s^{-1}$ and 13.9 $cm \cdot s^{-1}$, in the center and along the south-eastern edge, respectively.

Figure 7 presents the superposition of the kinetic energy field and the bed shear stress vectors computed within the two-channel harbor configuration under the four prevailing winds, also taking into consideration the water circulation inside the Canale Trasverso and the Fossa Traiana. Table IV compares the maximum values of bed shear stress and kinetic energy reached at different locations within the harbor, depending on the wind direction. The results show that in the new two-channel configuration, the dominant SW 247° wind presents similar values of kinetic energy compared to the previous one-channel configuration, in the central and eastern harbor basins, but induces decreasing values of energy in the entire western harbor basin (Figure 7A). Moreover, the results show that both the S 180° and SE 135° winds induce similar patterns characterized by maximum kinetic energies still located in the central harbor basin along the western side of the central pier, but also in the vicinity of the north-eastern channel and across the north-western harbor basin, a new pattern compared to the previous one-channel configuration (Figure 7B and C). In addition, the NE 22° wind here induces a large area of high kinetic energies that spreads across the entire harbor from the south-western channel to the north-eastern channel, which did not exist in the previous one-channel configuration (Figure 7D). Table IV shows that the highest values of bed shear stress (kinetic energy) always occur in the north-eastern harbor basin in the vicinity of the north-eastern channel for each wind direction, ranging from 93.6 $cN \cdot m^{-2}$ (91.3 $J \cdot m^{-3}$) under the NE 22° wind to 28.4 $cN \cdot m^{-2}$ (26.5 $J \cdot m^{-3}$) under the SW 247° wind. Thus, the results presented in Figure 7 and Table IV show that the operational north-eastern channel reinforces sediment erosion in the north-eastern sector of the harbor basin, with enlarged patches of higher energies compared to the previous one-channel configuration (Figure 5 and Table II), whatever the wind direction, which accounts for 61.3% of the summer period and 68% of the winter period. Moreover, comparisons between Figures 5 and 7 (Tables II and IV) demonstrate that the operating north-eastern channel has a limited impact on sediment erosion in the central harbor basin, and especially within the central channel, leading to the inner landing basins, under the SW 247°, S 180°, and SE 135° winds; but more specifically, the NE 22° wind induces the values of energy to increase 2.5-fold in the central channel in the two-channel configuration (69.6 $J \cdot m^{-3}$) compared to the one-channel configuration (27.5 $J \cdot m^{-3}$). Thus, the central channel presents, with the operational north-eastern channel, a new context of high energy that prevents access to the inner basins and affords protection from the risk of sediment infilling, under the S 180°, SE 135°, and NE 22° winds, accounting for 21% of the summer period and 51.3% of the winter period (Figure 6B, C, and D). These situations are associated with increasing inflows from the Canale Trasverso up to 14.5 and 18.3 $cm \cdot s^{-1}$ under the S 180° and SE 135° winds, respectively, as well as an increasing outflow of up to 11.7 $cm \cdot s^{-1}$ into the Canale Trasverso under the NE 22° wind. However, access to the inner basins still presents a high risk of sediment infilling under the dominant SW 247° wind (Figure 6A), accounting for 16.7% of the winter period and 40.3% of the summer period, associated with a outflowing current into the Canale Trasverso of 3.8 $cm \cdot s^{-1}$. Finally, Figure 7 and Table IV confirm that the operating north-eastern channel induces within the western harbor basin the lowest values of bed shear stress (kinetic energy) under each wind direction, ranging in the north-western harbor basin sector from 11.0 $cN \cdot m^{-2}$ (18.0 $J \cdot m^{-3}$) under the S 180° wind to 0.1 $cN \cdot m^{-2}$ (0.1 $J \cdot m^{-3}$) under the SW 247° wind. More specifically, the results show a drastic drop of the values of bed shear stress (kinetic energy) in the south-western harbor under each wind direction, ranging from 3.69 $cN \cdot m^{-2}$ (5.6 $J \cdot m^{-3}$) under the NE 22° wind to 0.57 cN m^{-2} (0.9 $J \cdot m^{-3}$) under the SW 247° wind. Thus, with the operating north-eastern channel, sediment infilling is maintained in the north-western harbor basin for 40.3% of the summer period and 44.2% of the winter period, and is particularly reinforced in the south-western harbor basin for 61.3% of the summer period and 68% of the winter period.

DISCUSSION

This multidisciplinary study provides new insights into the dynamics of water and sediment throughout the harbor of Portus. The numerical model enables theoretical removal and recovery of the north-eastern channel, leading to new interpretations concerning the impact of this channel on the prevention of sediment infilling of the inner harbor installations.

First, the results confirm that the one-channel harbor configuration, "artificially" observed through the model and characterized by weak hydrodynamics, may have functioned as a sediment trap, in relation to the south–north Tiber-induced sediment transit along the coast. The results demonstrate that the wind-induced circulation patterns within the one-channel harbor configuration present, under all the wind situations considered, eddy currents associated with low kinetic energy values that promote sediment deposition, especially in the western harbor basin (Figure 4 and Table I). Moreover, although the model respects an overall equilibrium in term of water masses flowing in and flowing out through the channel, according to the steady state of the numerical solution, the results demonstrate a highly contrasted spatial distribution of the bed shear stress and kinetic energy values that are high through the channel and much lower within the harbor basin (Figure 5 and Table II). Thus, these contrasted situations in term of sediment dynamics between the channel and the inner harbor basin suggest that the sediment budget is not equilibrated at the spatial scale of the harbor basin. This could be characterized by an efficient sediment loading through the channel, followed by a rapid sediment deposition within the harbor basin characterized by very low kinetic energy levels, especially near the center of each wind-induced eddy.

The results also showed that the opening of the north-eastern channel dramatically reinforces water circulation and sediment transit across the entire harbor between the two channels, with an increase in current (Figure 6B, C, and D and Table III) and kinetic energy values (Figure 7B, C, and D and Table IV), especially throughout the central and the north-eastern harbor basins under the S 180°, SE 135°, and NE 22° winds. It is interesting to note that the NE 22° winter wind promotes a new east–west circulation with higher kinetic energies across the western harbor basin, which does not exist in the one-channel configuration (Figures 5D and 7D and Tables II, IV). These results confirm that the north-eastern harbor basin and the north-eastern pass remain a zone characterized by high hydrodynamic levels with good conditions for sediment resuspension, rendering the north-eastern channel practicable for navigation over the long-term. However, the results confirm that weak hydrodynamic conditions, leading to sediment deposition, still prevail throughout the entire western harbor basin, and even become locally weaker compared to the previous one-channel configuration. It is noteworthy that the most frequent SW 247° wind, accounting for 40.3% of the summer period and 16.7% of the winter period, induces a strong lack of communication between the western harbor basin and offshore areas, associated with weak currents and very low levels of kinetic energy, even though the two channels are operating; this reinforces the persistent isolation of the western harbor basin and its overall positive sediment budget. It is interesting to note that weaker hydrodynamic conditions through the western passage of the harbor basin, more favorable for navigation, are induced by the SW 247° wind that prevails in summer, at the peak period of harbor activity. Also, the energetic hydrodynamic conditions (and resulting sediment erosion) computed in the model for the area along the eastern shore and the northern breakwater are confirmed by the coarse granulometry of the sediment particles measured in the several cores that have been taken in these zones (Goiran et al., 2007, 2009). Laser microgranulometric analysis shows that the sediments are very well-sorted evidence for the presence of currents. Macrofauna taxa indicate a high percentage of rheophilic species that grow in the flow of currents (Goiran et al., 2011a).

In general, our results confirm persistent conditions for sediment infilling within the western harbor basin, even when the north-eastern channel is operating, accounting for 61.3% of the summer period and 40.3% and up to 68% and 44.2% of the winter period, in the south-western and north-western harbor basins, respectively. In addition, the results indicate contrasted hydrodynamic conditions in this western harbor basin characterized by juxtaposed patches of low or high energy on a small-scale. We suggest that the overall context of sediment deposition associated with heterogeneous hydrodynamic conditions, unfavorable for navigation in the western harbor basin (the so-called Claudian offshore basin), may have influenced progressive adaptation of harbor activities to the advantage of the eastern harbor basin. It is probable that the harbor of Portus did not operate for a long period using only the western channel, thus indicating the importance of the north-eastern channel to ensure the maintenance of good conditions for navigation over the long-term.

Second, comparisons between both configurations considered in the model demonstrate the impact of the north-eastern channel in strengthening energy in the central harbor basin, thus preventing rapid sediment infilling of the central channel leading to the inner landing installations located close to the hexagon (Figures 5 and 7). Higher levels of kinetic energy in the central

harbor basin, beneficial to navigation in the central channel, only occur under the S 180° and SE 135° winds when the north-eastern channel is closed (Figure 5B and C), accounting for 21% of the summer period and 23.8% of the winter period; however, it occurs under the S 180°, SE 135°, and NE 22° winds when the north-eastern channel is operating (Figure 7B, C, and D), which accounts for 21% of the summer period and 51.3% of the winter period. The results indicate that the risk of sediment deposition in the central channel remains high under the most frequent SW 247° wind, whatever the configuration; this leads to the conclusion that access to the inner landing installations, with both channels operating, presents a risk of sediment infilling during 40.3% of the summer period and 16.7% of the winter period. Thus, improvement of access to the landing installations provided by the north-eastern channel may have occurred mostly in the winter period.

It is noteworthy that the results confirm weak hydrodynamic conditions and low energies within the channels of the inner basins, close to the landing installations and the hexagon (Figures 6 and 7). This result is consistent with the very fine sediment particles (silt and clay) measured in the several cores taken from these zones (Goiran et al., 2007, 2009, 2010, 2011).

Third, it is interesting that the model shows a two-way circulation inside the Canale Trasverso and the Fossa Traiana, which depending upon the wind. Both the S 180° and SE 135° winds induce inflowing currents from offshore to the inner basins, with reinforced velocities up to 18 $cm{\cdot}s^{-1}$ in the Canale Trasverso when the north-eastern channel is operating; inversely, both the SW 247° and NE 22° winds induce outflowing currents from the inner basins to offshore areas with reinforced velocities up to 12 $cm{\cdot}s^{-1}$ when the north-eastern channel is operating. It is to be noted that this efficient and reversible connection between the inner harbor and the open sea, allowing seawater inputs to the inner basins, may have contributed to the prevention of sediment infilling of the inner landing installations, which are considered to have been the most vulnerable area of the harbor of Portus. It is also interesting that the marine influence due to the frequent inflows of seawater suggested by the model is confirmed by the presence of numerous posidonia and marine shells in the sediment of the Canale Trasverso, as seen in several cores from this zone (Salomon et al., 2012).

CONCLUSIONS

The results of this modeling study have highlighted some fine-scale processes involved in the hydrosedimentary functioning of the harbor of Portus, which has led to a quantitative analysis of the impact of the north-eastern channel and the Canale Trasverso on the prevention of rapid sediment infilling of the inner landing installations. The prevention of sediment deposition in harbor basins was certainly a major challenge for engineers in Antiquity (Goiran & Morhange, 2003; Marriner & Morhange, 2006; Morhange & Marriner, 2009). This modeling of the harbor of Portus, in relation to the impact of a secondary channel on navigation within the basins, is similar to the previous study that we conducted on the ancient harbors of Alexandria, in relation to the major impact of the Heptastadion in the protection of harbor installations from sediment infilling (Millet & Goiran, 2007). These results encourage the use of numerical models in future studies of ancient harbors, for large basins as well as for small inner structures.

We particularly thank the reviewers for their helpful comments and suggestions for improving the manuscript. We also thank Cécile Vittori-Villette for her aid in the final design of the figures, and Elizabeth Willcox for reviewing and improving the English. We acknowledge all the institutions that supported this research: Ecole Française de Rome, Soprintendenza Speciale per i Beni Archeologici di Roma—Sede di Ostia (C. Morelli, L. Paroli, A. Pellegrino, A. Gallina Zevi), Maison de l'Orient et de la Méditerranée, Institut Méditerranéen d'Océanologie, Aix-Marseille Université, Université de Lyon, OMEAA platform, ARTEMIS-SHS program and radiocarbon laboratory of Lyon, Labex IMU, Portus Project, and ANR Young Scientist "Pol-Tevere."

REFERENCES

Arnoldus-Huyzendveld, A. (2005). The natural environment of the Agro Portuense. In S. Keay, M. Millett, L. Paroli & K. Strutt (Eds.), Portus, an archaeological survey of the port of imperial Rome (pp. 14–30). Rome: The British School at Rome.

Bellotti, P., Calderoni, G., Carboni, M.G., Bella, L.D., Tortora, P., Valeri, P., & Zernitskaya, V. (2007). Late quaternary landscape evolution of the Tiber River delta plain (Central Italy): New evidence from pollen data, biostratigraphy and 14C dating. Zeitschrift für Geomorphologie, 51, 505–534.

Bellotti, P., Calderoni, G., Rita, F.D., D'Orefice, M., D'Amico, C., Esu, D., Magri, D., Martinez, M.P., Tortora, P., & Valeri, P. (2011). The Tiber River delta plain (Central Italy): Coastal evolution and implications for the Ancient Ostia Roman settlement. The Holocene, 21, 1105–1116.

Boetto, G. (2010). Le port vu de la mer: l'apport de l'archéologie navale à l'étude des ports antiques. In S. Keay & G. Boetto (Eds.), Portus, Ostia and the Ports of the Roman Mediterranean (pp. 112–128). Rome: Contributions from Archaeology and History, Ministero per i Beni e le Attività Culturali.

Di Bella, L., Bellotti, P., Frezza, V., Bergamin, L., & Carboni, M.G. (2011). Benthic foraminiferal assemblages of the imperial harbor of Claudius (Rome): Further paleoenvironmental and geoarcheological evidences. The Holocene, 21, 1245–1259.

Fea, C. (1824). Alcune osservazioni sopra gli antichi porti d'Ostia, ora di Fiumicino. Roma: Presso Lino Condetini.

Giraudi, C., Paroli, L., Ricci, G., & Tata, C. (2006). Portus (Fiumicino—Roma): Il colmamento sedimentario dei bacini del Porto di Claudio e Traiano nell'ambito dell'evoluzione ambientale tardoantica e medievale del delta del Tevere. Archeologia Medievale, 33, 49–60.

Giraudi, C., Tata, C., & Paroli, L. (2009). Late Holocene evolution of Tiber river delta and geoarchaeology of Claudius and Trajan Harbor, Rome. Geoarchaeology, 24, 371–382.

Goiran, J.P., & Morhange, C. (2003). Géoarchéologie des ports antiques de Méditerranée: Problématiques et études de cas. Topoï, 11, 645–667.

Goiran, J.P., Ognard, C., Tronchère, H., & Canterot, X. (2007). Géoarchéologie du port antique de Rome: Problématiques, approche méthodologique et premiers résultats paléo-environnementaux. In: M. Bourgou (coord.) Les littoraux entre nature et sociétés Actes du colloque international de Tunis, 11–13 septembre 2006, publications de l'ENS et des éditions Sahar. Actes du Colloque International en l'Hommage au Pr. R. Paskoff sur les paléoenvironnements littoraux (pp. 201–225), Université de Tunis.

Goiran, J.P., Tronchère, H., Collarelli, U., Salomon, F., & Djerbi, H. (2009). Découverte d'un niveau marin biologique sur les quais de Portus: le port antique de Rome. Méditerranée, 112, 59–67.

Goiran, J.P., Tronchère, H., Salomon, F., Carbonel, P., Djerbi, H., & Ognard, C. (2010). Palaeoenvironmental reconstruction of the ancient harbors of Rome: Claudius and Trajan's marine harbors on the Tiber delta. Quaternary International, 216, 3–13.

Goiran, J.P., Salomon, F., Tronchère, H., Djerbi, H., Carbonel, P., Ognard, C., & Oberlin, C. (2011a). Géoarchéologie des ports de Claude et de Trajan, Portus, delta du Tibre, MEFRA, 18, 157–236.

Goiran, J.P., Salomon, F., Tronchère, H., Carbonel, P., Djerbi, H., & Ognard, C. (2011b). Caractéristiques sédimentaires du bassin portuaire de Claude: nouvelles données pour la localisation des ouvertures. In S. Keay & L. Paroli (Eds.), Portus and its Hinterland (pp. 31–45). Archaeological Monographs of the British School at Rome, London.

Goiran, J.P., Salomon, F., Pleuger, E., Vittori, C., Mazzini, I., Boetto G., Arnaud, P., & Pellegrino A. (2012). Résultats préliminaires de la première campagne de carottages dans le port antique d'Ostie. Chroniques des Mélanges de l'Ecole Française de Rome, 123, 2–7.

Goiran, J.P., Salomon, F., Mazzini, I., Bravard, J.P., Pleuger, E., Vittori, C., Boetto, G., Christiansen J., Arnaud, P., Pellegrino, A., Pepe, C., & Sadori, L. (2014). Geoarchaeology confirms location of the ancient harbour basin of Ostia (Italy). Journal of Archaeological Science, 41, 389–398.

Heinzelmann, M., & Martin, A. (2002). River port, navalia, and harbour temple at Ostia: New results of a DAI-AAR Project. Journal of Roman Archaeology, 15, 5–19.

Keay, S., & Paroli, L. (2011). Portus and its hinterland: Recent archaeological research. London: British School at Rome.

Keay, S., Millet, M., Paroli, L., & Strutt, K. (2005). Portus: An archaeological survey of the port of Imperial Rome. London: Collection of the British School at Rome.

Le Gall, J. (1957). Le Tibre, fleuve de Rome dans l'antiquité, Paris: Pr. Univ. De France.

Lugli, G., & Filibeck, G. (1935). Il Porto di Roma imperiale e l'Agro Portuense, Roma: Office dell'Istituto Italiano d'Arti Grafiche.

Marriner, N., & Morhange, C. (2006). Geoarchaeological evidence for dredging in Tyre's ancient harbor, Levant. Quaternary Research, 65, 164–171.

Marriner, N., Morhange, C., & Goiran, J.P. (2010). Coastal and ancient harbour geoarchaeology. Geology Today, 26, 21–27.

Mazzini, I., Faranda, C., Giardini, M., Giraudi, C., & Sadori, L. (2011). Late Holocene palaeoenvironmental evolution o the ancient harbour of Portus (Latium, Central Italy). Journal of Palaeolimnology, 46, 243–256.

Millet, B., & Goiran, J.P. (2007). Impacts of Alexandria's Heptastadion on coastal hydro-sedimentary dynamics during the Hellenistic period: A numerical modelling approach. International Journal of Nautical Archaeology, 36, 167–176.

Millet, B., Blanc, F., & Morhange, C. (2000). Modélisation numérique de la circulation des eaux dans le Vieux-Port de Marseille vers 600 ans avant J.-C. Méditerranée, 1-2, 61–64.

Morelli, C., Marinucci, A., & Arnoldus-Huyzendveld, A. (2011). Il Porto di Claudio: nuove scoperte, in Portus and its Hinterland, recent archaeological research, In Simon Keay & Lidia Paroli (eds), Archaeological Monographs of the British School at Rome, pp. 47–65.

Morhange, C., & Marriner, N. (2009). Roman dredging in ancient Mediterranean harbours. Bollettino di Archeologia Online, vol. spe. IAAC, 42, 23–32.

Özdaş, H., & Kızıldağ, N. (2013). Archaeological and geophysical investigation of submerged coastal structures in Kekova, southern coast of Turkey. Geoarchaeology, 28, 504–516.

Pepe, C., Giardini, M., Giraudi, C., Masi, A., Mazzini, I., & Sadori, L. (2012). Plant landscape and environmental changes recorded in marginal marine environments: The ancient Roman harbour of Portus (Rome, Italy). Quaternary International, 303, 73–81.

Pomey, P. (1982). Le navire romain de la Mandrague de Giens. CRAI, 4, 133–154.

Pomey, P. (1997). La navigation dans l'Antiquité. Aix-en-Provence: Edisud.

Pomey, P., & Tchernia, A. (1978). Le tonnage maximum des navires de commerce romains. Archaeonautica, 2, 233–251.

Sadori, L., Giardini, M., Giraudi, C., & Mazzini, I. (2010). The plant landscape of the imperial harbour of Rome. Journal of Archaeological Science, 37, 3294–3305.

Salomon, F., Delile, H., Goiran, J.P., Bravard, J.P., & Keay, S. (2012). The Canale di Comunicazione Traverso in Portus: The Roman sea harbour under river influence (Tiber delta, Italy), Géomorphologie: Relief, Processus, Environnement, 1, 75–90.

Stanley, J.D., & Bernasconi, M.P. (2012). Buried and submerged Greek archaeological coastal structures and artifacts as Gauges to measure late Holocene seafloor subsidence off Calabria, Italy. Geoarchaeology, 27, 189–205.

Testaguzza, O. (1970). Portus :Illustrazione dei porti di Claudio e Traiano e della città di Porto a Fiumicino. Rome: Julia editrice.

Zevi, F. (2001). Les débuts d'Ostie. In J.P. Descoeudres (Ed.), Ostia, port et porte de la Rome antique (pp. 3–9). Genève: Georg.

